euspen's 26th International Conference & Exhibition, Krakow, PL, June 2026
www.euspen.eu

Ultrafast laser fabrication of transparent superhydrophobic silica glass for optical window applications

Kai Liao[1], Chi Fai Cheung[1,*], Chunjin Wang[1]

[1]*State Key Laboratory of Ultra-precision Machining Technology, Department of Industrial and Systems Engineering, The Hong Kong Polytechnic University, Hung Hom, Kowloon, Hong Kong, China.*

**Corresponding author: benny.cheung@polyu.edu.hk*

Abstract

Transparent and durable superhydrophobic surfaces are critical for optical window applications. Inspired by the water-responsive transparency of Hydrangea hirta leaves, this paper presents a novel femtosecond laser processing method using a temporally shaped dual-pulse approach to fabricate large-area superhydrophobic silica glass surfaces with high optical transparency. By temporally shaping the laser pulses and adjusting the energy distribution, free-electron dynamics were precisely controlled to form uniform hierarchical micro/nanostructures, promoting dense nanowire and nanoparticle growth, enhancing the hierarchical structure, and facilitating superhydrophobicity. These structures stabilize a Cassie–Baxter wetting regime and minimize optical scattering. By using a single-scan, maskless process, a 1.5 × 1.5 cm² sample was fabricated in 75 seconds, demonstrating rapidity and scalability of the method. After fluorocarbon coating, the surface exhibited a water contact angle of 154.5° and optical transmittance above 88% in the 300–800 nm range. Surface analysis revealed a high CF_2/CF_3 ratio correlating with enhanced hydrophobicity. The surfaces also showed excellent mechanical, thermal, and chemical durability. More importantly, they appear translucent in air and become highly transparent underwater, with optical transmittance exceeding 90%. This work provides a rapid, scalable, and versatile method to produce transparent, durable, superhydrophobic silica glass surfaces for optical windows, self-cleaning coatings, anti-fouling surfaces, and smart optical devices.

Keywords: Ultrafast laser processing; Temporal pulse shaping; Silica glass; Superhydrophobic surface; Optical window applications

1. Introduction

Transparent optical components are widely used in optical windows [1], imaging systems [2], and sensing applications [3], where high optical transmittance is maintained under complex environmental conditions. However, conventional glass surfaces are easily contaminated by water droplets, dust, and organic pollutants, leading to optical degradation and reduced reliability.

Superhydrophobic surfaces, characterized by water contact angles exceeding 150°, provide an effective route to address this issue due to their water repellency and self-cleaning capability [4-6]. In such surfaces, droplets remain in a Cassie–Baxter (C-B) state, where trapped air pockets reduce the solid–liquid contact area and facilitate droplet removal [7]. However, achieving superhydrophobicity on transparent substrates remains challenging, as the micro/nanostructures required for water repellency often introduce strong light scattering, thereby reducing optical transparency. In addition, conventional fabrication methods, such as chemical etching and coating-based approaches, typically involve multi-step processes and limited controllability [8-10].

Femtosecond laser processing offers a promising solution for direct structuring of transparent materials, enabling localized energy deposition and flexible patterning without masks [11]. Various micro/nanostructures can be generated to modify surface wettability. Nevertheless, controlling the structural morphology to simultaneously achieve high hydrophobicity and high optical transparency remains a key challenge, particularly when balancing structure depth, feature size, and processing efficiency. To address these challenges, a microgroove-based surface architecture is proposed in this study, aiming to minimize the solid–liquid contact fraction while limiting the modified area to preserve optical clarity. A single-scan femtosecond laser strategy is employed to improve fabrication efficiency, and a temporally shaped dual-pulse approach is further introduced to enhance energy deposition and promote the formation of hierarchical micro/nanostructures.

The resulting surfaces exhibit high water contact angles, low adhesion, and high optical transmittance. This study demonstrates a controllable and scalable approach for fabricating transparent superhydrophobic surfaces, providing potential applications in optical windows, anti-fouling coatings, and advanced photonic devices.

2. Materials and methods

2.1. Materials

Commercial fused silica glass substrates with dimensions of 20 mm × 20 mm × 1 mm were used as the base material. Prior to laser processing, the samples were ultrasonically cleaned sequentially in acetone, ethanol, and deionized water for 10 min each to remove surface contaminants.

2.2. Methods

Surface structuring was performed using a femtosecond laser system with a central wavelength of 1030 nm and a pulse duration in the femtosecond regime. The laser beam was focused onto the silica surface through a galvanometer scanning system. The sample was mounted on a computer-controlled three-axis translation stage. To regulate energy deposition during laser–matter interaction, temporal pulse shaping was employed to tailor the energy distribution.

During processing, the laser beam scanned across the surface in a raster pattern. The scanning parameters, including pulse energy, scanning speed, and scanning interval, were optimized

to produce uniform hierarchical structures. The fabrication process was completed in a single-pass scanning strategy, enabling rapid large-area patterning. After laser structuring, the samples were treated with a fluorocarbon-based coating to reduce the surface energy. The coating was applied via vapor-phase deposition, forming a thin hydrophobic layer on the hierarchical structures.

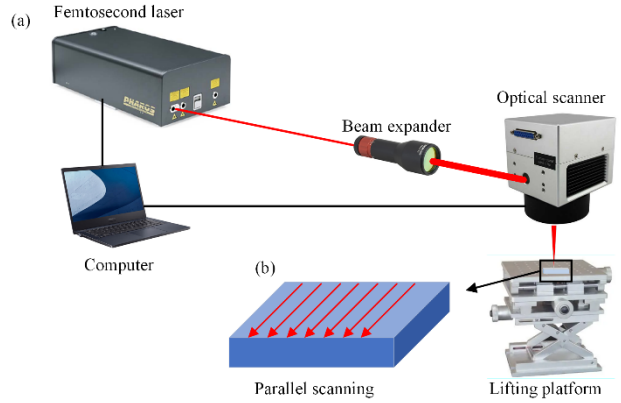

Figure 1. Schematic of the femtosecond laser processing setup: (a) optical configuration; (b) parallel scanning path.

2.3. Characterization

Surface morphology was characterized by scanning electron microscopy (SEM) and laser scanning confocal microscopy (LSCM). Surface wettability was evaluated by measuring the static water contact angle using a contact angle goniometer. The dynamic wetting behavior of water droplets was recorded using a high-speed camera. Optical transmittance was measured using a UV–visible spectrophotometer over the wavelength range of 300–800 nm. The surface chemical composition was analyzed by X-ray photoelectron spectroscopy (XPS), with particular focus on the relative contents of CF_2 and CF_3 groups. Mechanical durability was assessed through repeated abrasion tests, while thermal stability was evaluated by heating the samples at elevated temperatures. Chemical resistance was examined by exposure to acidic and alkaline solutions.

3. Results and Discussion

3.1. Design of superhydrophobic microstructures via single-scan processing

To achieve a balance between superhydrophobicity, optical transparency, and fabrication efficiency, an one-dimensional microgroove-based surface architecture was designed using a single-scan femtosecond laser processing strategy. The designed structure consists of periodically arranged microgrooves with controlled groove width (a), spacing (d), and depth (h), forming a composite solid–air interface that supports a stable C–B wetting state. The apparent contact angle is governed by the solid–liquid contact fraction (f_s), which can be approximated as $f_s = a/d$. As a result, minimizing f_s is essential for enhancing surface hydrophobicity [12].

From a structural design perspective, reducing the groove width or increasing the spacing can effectively decrease f_s. However, excessive spacing may lead to an increase in the effective ridge width due to laser–material interaction effects, thereby increasing the contact fraction. This introduces a trade-off, requiring an optimized spacing to balance contact reduction and structural fidelity. In addition to lateral parameters, the groove depth (h) plays a critical role in maintaining a stable C–B state. insufficient depth may result in liquid penetration and transition to the Wenzel state. As a result, the groove depth must exceed a critical value (hcr) to ensure the stability of the air-trapped interface [13].

Considering the laser spot size (~30 μm), the achievable groove width is constrained to the same order of magnitude. Consequently, the structural design primarily focuses on optimizing the spacing (d) to control groove overlap and fs. a spacing of 30 μm enables well-defined groove formation with sufficient depth while maintaining a reduced contact fraction.

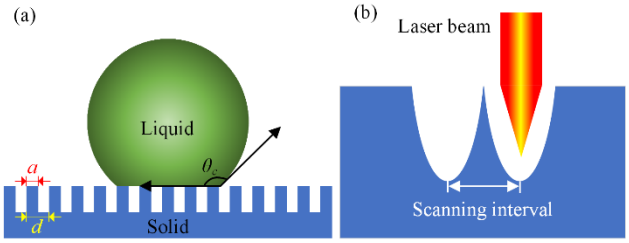

Figure 2. (a) Schematic illustration of droplet behavior in the C–B state. (b) microgroove formation under laser ablation.

3.2 Fabrication of microgroove structures via single- and dual-pulse laser ablation

To realize the designed microgroove structures, femtosecond laser ablation was first performed using a single-pulse scanning strategy to establish a baseline process window. By adjusting scanning speed and pulse energy, uniform microgroove arrays could be obtained under optimized conditions (80 μJ pulse energy, 100mm/s scanning speed,). However, despite achieving well-defined microstructures, the resulting surface exhibited a water contact angle of 145.8° after chemical modification (Fig.6a), which is below the superhydrophobic threshold.

To overcome this limitation, a dual-pulse laser strategy was introduced to enhance energy deposition. The dual-pulse sequences, generated using the burst mode of the laser system, consisted of two sub-pulses separated by ~20 ns. Three energy distribution modes—2:3 (Type 1, low–high), 1:1 (Type 2, equal), and 3:2 (Type 3, high–low)—were investigated at a constant total pulse energy of 80 μJ.

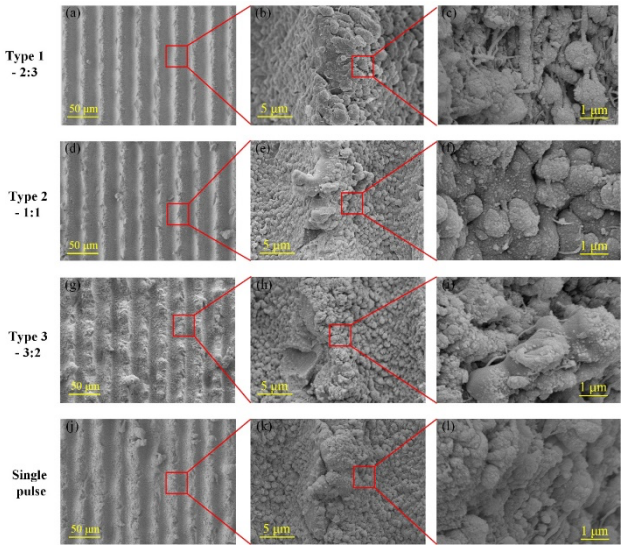

Figure 3. SEM of surface morphologies under different pulse modes. (a–c) Type 1; (d–f) Type 2; (g–i) Type 3; (j–l) single-pulse.

Compared with the single-pulse mode, the dual-pulse strategy significantly modified the resulting surface morphology. As shown in Fig. 3, the low–high sequence (Type 1) produced

uniform microgrooves with well-preserved ridge structures, accompanied by a dense distribution of nanoscale features, including nanoparticles and nanowire-like structures. These hierarchical micro/nanostructures are beneficial for enhancing surface roughness and promoting air entrapment. In contrast, Type 2 generated moderately developed nanostructures, while Type 3 resulted in irregular grooves with sparse nanoscale features. In addition to the improved nanoscale morphology, the dual-pulse strategy also enhanced the ablation depth. As shown in Fig. 4, the groove depth reached 16.8 μm for Type 1, which exceeds the critical depth required to maintain a stable Cassie–Baxter state (Fig.4).

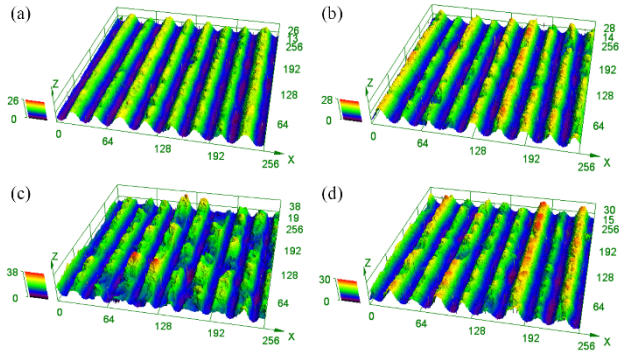

Figure 4. LSCM surface morphologies and under different pulse modes: (a) Type 1; (b) Type 2; (c) Type 3; (d) Single-pulse.

The superior performance of the low–high dual-pulse configuration can be attributed to the temporal modulation of energy deposition. As shown in Fig. 5, the initial low-energy pulse preconditions the surface, reducing reflectivity and plasma shielding, thereby enhancing the absorption of the subsequent high-energy pulse. This staged energy delivery facilitates more efficient material removal and promotes the formation of hierarchical structures.

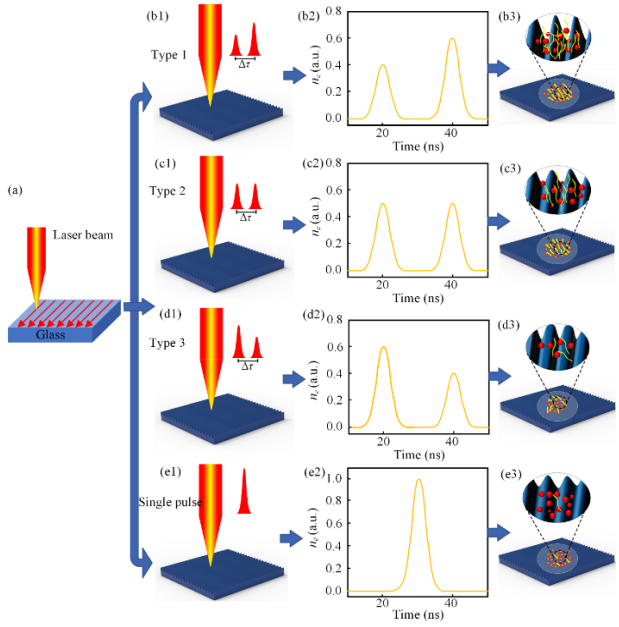

Figure 5. Schematic illustration of surface micro/nanostructure formation under various pulse modes.

On the whole, the low–high configuration (Type 1), enables the simultaneous formation of deeper microgrooves and richer nanoscale features. This synergistic enhancement of structure depth and hierarchical morphology provides a robust foundation for achieving stable superhydrophobicity in subsequent surface functionalization.

3.3. Performance evaluation of laser-fabricated surfaces

The functional performance of the optimized laser-fabricated surface was evaluated in terms of wettability, optical transparency, chemical composition, and stability.

3.3.1 Static wettability

The optimized surface exhibits a water contact angle of 154.5° after fluorination, indicating a stable Cassie–Baxter wetting state and superhydrophobic behavior. A low sliding angle of 2.8° further confirms minimal droplet adhesion (Fig. 6b).

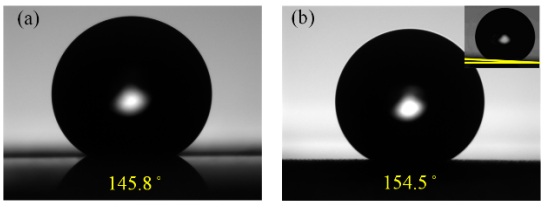

Figure 6. Static WCAs for surfaces under different pulse modes: (a) single-pulse. (b)Type 1 (with water sliding angle).

3.3.2 Dynamic wettability

Dynamic wettability was evaluated using droplet impact tests. The droplets spread upon impact and rapidly recoiled, bouncing off the surface without fragmentation. Multiple rebounds were observed, indicating low adhesion (Fig. 7).

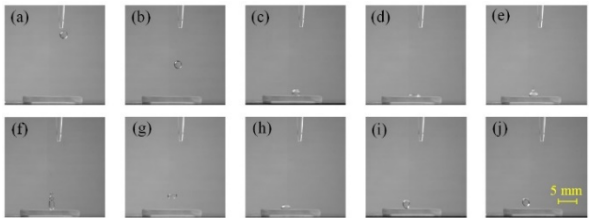

Figure 7. High-speed imaging of droplet impact dynamics on the laser-fabricated superhydrophobic glass surface.

3.3.3 Optical transparency

The optimized surface maintains a high optical transmittance of 88.78% in the visible range, compared to 93.23% for untreated glass. After surface fluorination, the transmittance remains at 87.67%.

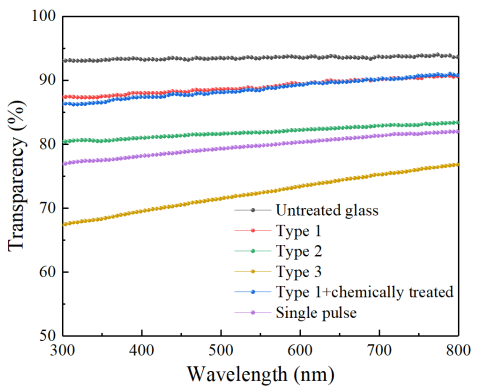

Figure 8. Comparison of optical transmittance in the visible wavelength range for samples processed under different pulse configurations.

3.3.4 Chemical composition

XPS analysis confirms the formation of a fluorinated surface layer with a high content of low-surface-energy functional groups, particularly $–CF_3$ species. This chemical composition contributes to reduced surface energy and plays a key role in achieving superhydrophobicity.

3.3.5 Stability and robustness

The optimized surface demonstrates excellent mechanical and environmental stability. The C-B state remains stable under droplet compression, and repeated tape-peeling tests show negligible degradation in wettability. In addition, the surface maintains its performance under outdoor exposure, water jet impact, thermal treatment, and chemical immersion, confirming its durability for practical applications.

4. Applications

The transparent superhydrophobic surface fabricated via the dual-pulse femtosecond laser single-scan strategy exhibits coupled optical and wetting functionalities, which are particularly relevant for optical window applications. In air, the hierarchical micro/nanostructures induce strong light scattering, resulting in a frosted appearance. Upon exposure to water, refractive index matching between water and glass suppresses scattering, leading to a rapid transition to a transparent state.

As shown in Fig. 9, the Hydrangea hirta leaf shows a similar behavior, appearing opaque in air and becoming transparent after wetting. The laser-fabricated surface mimics this mechanism, switching from a translucent state in air to a highly transparent state underwater. Quantitative measurements indicate a transmittance of ~88% in air and ~90% in water, with only a minor reduction compared to untreated glass.

This environment-responsive optical behavior enables dynamic regulation of light transmission, allowing the surface to maintain high clarity under wet or submerged conditions. Such characteristics make it highly suitable for optical windows operating in humid, rainy, or underwater environments, where both transparency and contamination resistance are critical.

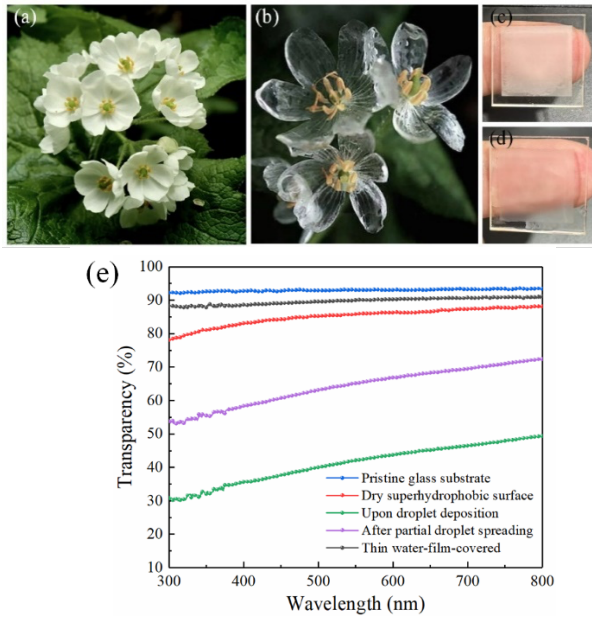

Figure 9. Bioinspired environment-responsive transparency：(a) Paraboea rufescens leaf in air (opaque); (b) after wetting (transparent); (c) laser-fabricated glass in air (frosted); (d) with water film (enhanced transparency); (e) transmittance comparison in air and underwater with untreated glass.

5. Conclusion

A femtosecond laser-based strategy was developed to fabricate transparent superhydrophobic microstructures on silica glass for optical window applications. By employing temporal pulse shaping, hierarchical micro/nanostructures composed of nanowires and nanoparticles were generated, enabling a stable Cassie–Baxter state with a water contact angle of 154.5° after surface modification.

High optical transparency was preserved despite surface structuring, with transmittance exceeding 88% in the visible range. Notably, the structured surface exhibited environment-responsive behavior, appearing translucent in air while achieving high transparency underwater (transmittance >90%) due to refractive index matching.

The process demonstrates high fabrication efficiency, enabling rapid patterning via a single-pass scanning strategy (1.5 × 1.5 cm^2 in 75 s), while maintaining good structural uniformity and durability. These results indicate a practical route for integrating superhydrophobicity and high optical performance in optical windows, with strong potential for self-cleaning and anti-fouling applications.

Acknowledgments

This work was supported by Innovation and Technology Commission (ITC) of the Government of the Hong Kong Special Administrative Region, China (ITS/609/24FP) and the postdoc matching fund of The Hong Kong Polytechnic University (Project Code: 1-W31V).

References

[1] Guan S, Li Y, Xu C, Yin N, Xu C, Wang C, Wang M, Xu Y, Chen Q, Wang D, Zuo L and Chen H 2024 Adv. Mater. **36** e2400342
[2] Zhao Z, Kuzhandaivel D, Zhou X, Zhang W, Yuan Y, Zhang G and Weng Z 2025 Prog. Org. Coat. **204** 109255
[3] Liao K, Wang W, Wang C and Cheung C 2025 ACS Appl. Mater. Interfaces **17** 17530–17542
[4] Liu Y, Moevius L, Xu X, Qian T, Yeomans J M and Wang Z 2014 Nat. Phys. **10** 515–519
[5] Li C, Wang F, Wang Y, Guo M, Li J, Deng C, Song F, Yang W and Wang Y 2025 Nat. Commun. **16** 2729
[6] Luo J and Guo Z 2024 Nanoscale 16 16404
[7] Liu Y, Zhang L, Hu J, Cheng B, Yao J, Huang Y and Yang H 2024 Surf. Coat. Technol. **477** 130352
[8] Zhang M and Li H 2025 Mater. Chem. Phys. **338** 130634
[9] Tong W, Wu Z and Xiong D 2023 Sustain. Mater. Technol. **37** e693
[10] Wang L, Liu M, Wu Y and Zheng H 2022 Nanomaterials **12** 4203
[11] Li K, Myers N, Bishop G, Li Y and Zhao X 2022 J. Manuf. Process. **79** 177–184
[12] Zhu J, Li W, Wang T, Feng H, Cheng J, Lin C, Wang X, Wang W and Chen S 2025 Chem. Eng. J. **505** 159218
[13] Liao K, Wang W, Mei X, Zhao W, Yuan H, Wang M and Wang B 2023 Mater. Des. **225** 111501